Chem

CellPress

Article

Dynamic Phenomena at Perovskite/Electron-Selective Contact Interface as Interpreted from Photovoltage Decays

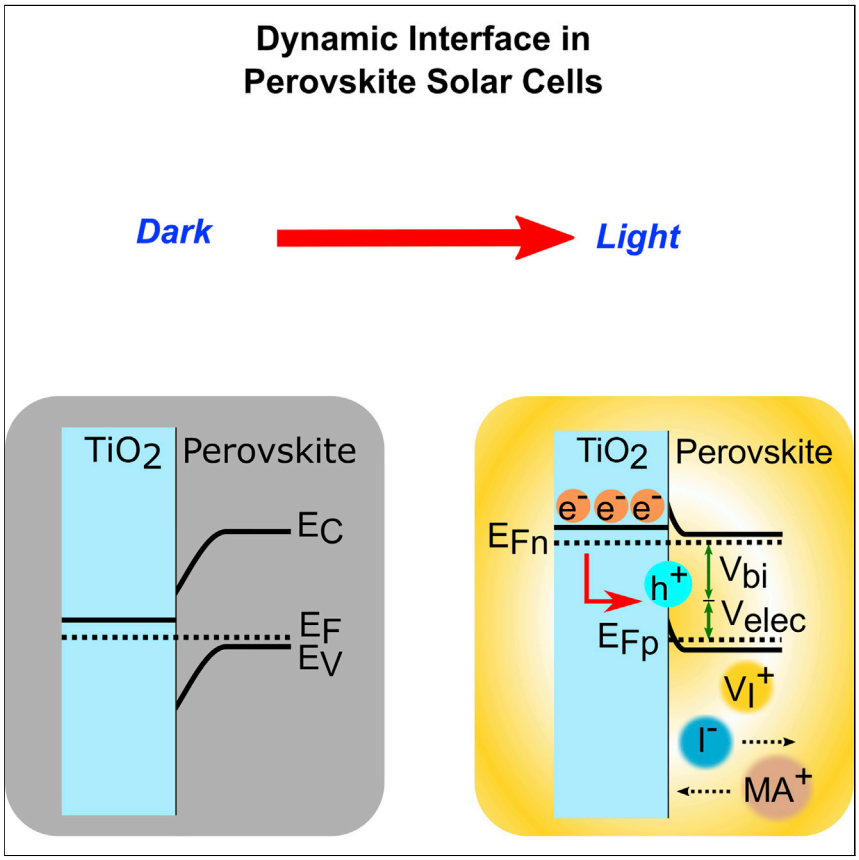

Bisquert and colleagues demonstrate the impact of positive charge accumulation at the electron contact of perovskite solar cells.

Ronen Gottesman, Pilar Lopez-Varo, Laxman Gouda, ..., Shay Tirosh, Arie Zaban, Juan Bisquert

arie.zaban@biu.ac.il (A.Z.)
bisquert@uji.es (J.B.)

HIGHLIGHTS

Charge accumulation at the contact determines the behavior of perovskite solar cells

Simulations show simultaneous accumulations of majority electronic carriers and ions

A slow responding electrostatic photopotential is formed at the accumulation region

Memory effect is caused by fast electron recombination and very slow ion drift

Gottesman et al., Chem 1, 776–789
November 10, 2016 © 2016 Elsevier Inc.
http://dx.doi.org/10.1016/j.chempr.2016.10.002

7 AFFORDABLE AND CLEAN ENERGY

CrossMark

Chem

CellPress

Article

Dynamic Phenomena at Perovskite/Electron-Selective Contact Interface as Interpreted from Photovoltage Decays

Ronen Gottesman,[1,4] Pilar Lopez-Varo,[2,4] Laxman Gouda,[1] Juan A. Jimenez-Tejada,[2] Jiangang Hu,[1] Shay Tirosh,[1] Arie Zaban,[1,*] and Juan Bisquert[3,5,*]

SUMMARY

Drastic changes in open-circuit voltage decay (OCVD) response time in $CH_3NH_3PbX_3$ perovskites have been systematically investigated in order to elucidate the dynamic properties of the interface. Under pre-illumination treatment, the decay times are reduced by orders of magnitude, but if left to rest for sufficient time, the solar cell evolves to its original decay kinetics. In order to explain these observations, we developed advanced modeling of the perovskite solar cell to obtain a realistic description of the immediate vicinity of the interface, including ionic variable concentration and accumulation of holes via degenerate statistics in the space charge region. The results reveal a large amount of majority carriers at the minority carrier extraction contact, assisted by additional ionic charge. The surface band bending related to accumulation gives an electrostatic contribution to the photovoltage in a manner governed by slow dynamics of cations at the electron-selective contact. The modeling of the interface allows us to describe the dynamics of the contact region dominated by surface charging and recombination. These phenomena also play an important role in operation conditions and current-voltage scans of the solar cell.

INTRODUCTION

Solar cell devices based on organic-inorganic halide perovskites have achieved high power conversion efficiencies of more than 22% over a short time span of 6 years and have revolutionized the field of photovoltaics. Despite that, $CH_3NH_3PbX_3$ perovskite solar cells suffer from critical changes in device performance under working conditions that impede further development for their commercialization as cheap and highly efficient materials in optoelectronic applications (here, we distinguish between the changes in device performance and the instability of the $CH_3NH_3PbX_3$ materials).

The changes in device performance manifest mainly by a current-voltage hysteresis,[1–3] which leads to unstable power outputs and additional photo- and electric-field-induced effects.[4–6] The magnitude of the performance changes is dynamic and usually depends on three parameters: (1) the working conditions, such as current-voltage scanning rate and illumination intensity; (2) pre-treatments prior to the current-voltage scan (light soaking and/or application of an electric field); and (3) the type of selective contacts interfaced with the perovskites to make the full device. The working conditions and the type of pre-treatments prior to measuring the solar cells are fairly indifferent to the device structure. However, the interface along

The Bigger Picture

The extraordinary properties of lead halide hybrid perovskite materials make them an ideal candidate to mark a revolution for new cheap, clean photovoltaic energy devices and innovative optoelectronic technologies. However, the actual devices often display uncontrolled fluctuations when submitted to external perturbation for measurement and operation. Here, we show that the interface plays a critical role in the random experimental response often observed in perovskite solar cells. When the contact interface where the metal oxide extraction layer meets the perovskite absorber is operated by light or voltage, it shows a memory effect by the formation of electric polarization and very short-range charge accumulation. The reason for this is the contrast time response between fast electron recombination and slow ion drift. An electrostatic component of the photovoltage associated with long response times has been identified.

the device plays a crucial role in determining device performance and is affected by the device structure and type of contact material (e.g., using TiO_2 versus [6,6]-phenyl-C61 butyric acid methyl ester [PCBM] as the n-type contact). An effective heterojunction is found to exist at the contact/perovskite interface, contributing to the relatively fast extraction of free electrons. However, some fundamental questions, including the interfacial atomic and electronic structures and the interface stability, need to be further clarified.[7] Understanding the interface in perovskite photovoltaics is tremendously important from the perspective of both the processing chemistry and the photophysics of the carriers, which are the key parameters for the photovoltaic behavior of the corresponding device.[7–9]

In recent years, many studies have focused on revealing fundamental insights about the electronic processes and photovoltaic mechanisms in perovskite materials and devices. Time transient measurements (i.e., probing the decay of electrical or optical properties) are very commonly used characterization techniques of photovoltaic devices. The transient measurements can shed light on fundamental mechanisms such as voltage and current generation and charge recombination in perovskite solar cells. These transient decays, such as open-circuit voltage decay (OCVD),[10] transient photovoltage decay (TPD), and transient absorption spectroscopy (TAS),[11,12] are generally interpreted in terms of electronic processes in a rigid lattice framework (i.e., the device structure and intrinsic properties do not change under working conditions or are affected by the measurement itself). However, because perovskites are considered to be mixed ionic-electronic conductors by nature, their crystal structure cannot be regarded as a rigid lattice framework.[13] Adding that to the established fact that device performance changes under illumination and electric fields until it reaches a new steady state,[6] we performed time transient measurements on full devices before and after pre-treatments. This will help develop a more in-depth understanding of the working mechanisms in operating perovskite solar cells.

Here, we studied the dynamic influence of light-soaking (1 sun intensity) pre-treatments in perovskites solar cells on photovoltage decay as well as the role of two different contact/perovskite interfaces by using OCVD spectroscopy. We observed gradual pronounced changes in the photovoltage decay as a function of light-soaking time, whereas the kinetics of the changes were affected by the type of selective contact interfaced with the perovskite. The changes were reversible, moving between light and dark pre-treatment conditions. Our results show that the contact/perovskite interface is critical and greatly affects photovoltage generation and decay. We formulated a model to study the effect of a distribution of mobile ions on the band bending and carrier distribution along a perovskite solar cell under illumination at open-circuit voltage. Furthermore, we witnessed the generation and decay of the electrostatic contribution to the photovoltage, which was also modeled to be governed by slow dynamics of cations at the electron-selective contact. We show that after light-soaking pre-treatments, OCVD characterizes mostly the contact/perovskite interface rather than the full device. This implies that pre-treatments significantly change the results of characterization techniques that use contacts, meaning that any techniques that measure a full device, and anyone measuring perovskite-based solar cells, must take this information into consideration.

RESULTS

In the past, we have performed OCVD measurements on a wide range of optoelectronic devices ranging from dye-sensitized solar cells[10] to perovskite solar cells.[14] The OCVD technique is considered to have certain advantages over frequency- or

[1]Department of Chemistry, Institute for Nanotechnology & Advanced Materials, Bar-Ilan University, Ramat Gan 52900, Israel

[2]Departamento de Electrónica y Tecnología de Computadores, CITIC-UGR, Universidad de Granada, 18071 Granada, Spain

[3]Institute of Advanced Materials (INAM), Universitat Jaume I, 12006 Castelló, Spain

[4]Co-first author

[5]Lead Contact

*Correspondence: arie.zaban@biu.ac.il (A.Z.), bisquert@uji.es (J.B.)

http://dx.doi.org/10.1016/j.chempr.2016.10.002

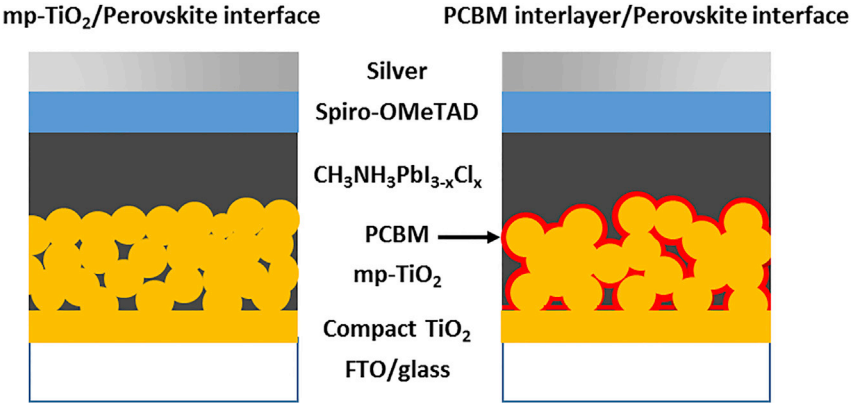

Figure 1. The Types of Perovskite Solar Cells Measured in the Study

A perovskite solar cell with an mp-TiO_2/perovskite interface (left) and an mp-TiO_2/PCBM interlayer/perovskite interface (right) was used for studying the role of the contact/perovskite interface on OCVD.

steady-state-based methods: (1) it provides a continuous reading of lifetime as a function of OCV, (2) it is experimentally much simpler, and (3) data treatment is extremely straightforward for obtaining the main quantities that provide information on the recombination mechanisms. However, there are still many uncertainties about the interpretation of the decays in perovskite solar cells, and in this study we addressed these by the following methodology. A typical experiment consisted of performing an OCVD measurement on a device that was stored in the dark overnight (labeled reference), followed by two consecutive measurement stages: (1) a light-soaking stage, during which OCVD was measured after light soaking for increasing times, and (2) a dark recovery stage, during which OCVD was measured after the light-soaking source was turned off in time intervals identical to the light-soaking time intervals.

In order to study the role of the selective contact interfaced with the perovskite, we fabricated two sets of devices with slightly different structures, modified only at the n-type contact. The structure of the first set was FTO/compact TiO_2/mp-TiO_2/$CH_3NH_3PbI_{3-x}Cl_x$/spiro-OMeTAD/Ag. In a recent study,[15] we presented the full structural, morphological, and optical characterization of our devices, which are similar to the devices used in this current work. For the second set of devices, we deposited a PCBM interlayer on top of mesoporous (mp)-TiO_2 after deposition of $CH_3NH_3PbI_{3-x}Cl_x$ and the rest of the devices' layers (Figure 1).

OCVD was measured by a home-built system consisting of an array of white LEDs as the light-soaking source, and a single red LED as the illumination source that generated the photovoltage. The measurements were conducted as follows: in the OCVD measurement, the solar cell was held at open-circuit voltage in the dark, and then the red LED was turned on (intensity equivalent to 0.1 sun, measured with a calibrated Si photodiode) until the photovoltage stabilized. For all measurements, the red LED illumination time was 1 s, which was sufficient for the photovoltage to rise and stabilize. When the red LED was turned off, the OCVD was recorded. In the light-soaking stage, the white LED array was turned on for prolonged illumination of the device (intensity equivalent to 1 sun) and was then turned off right before each OCVD measurement. All LEDs were cold light sources (see emission spectra in Figure S1A), and the temperature of the devices was verified with a thermocouple that was

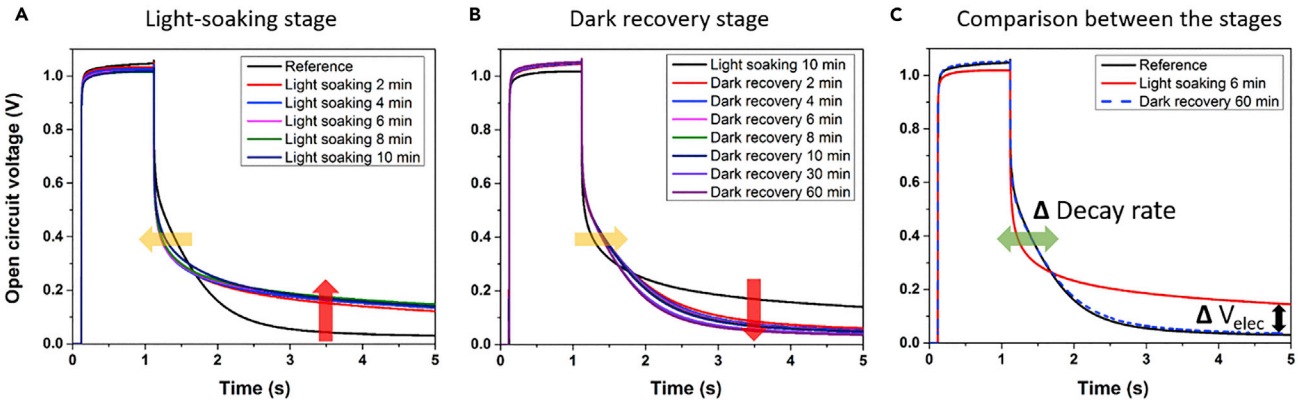

Figure 2. OCVD Data for a Perovskite Solar Cell with a $TiO_2/CH_3NH_3PbI_{3-x}Cl_x$ Interface

(A and B) Changes in the decay rate appear in the light-soaking stage (A) and slowly revert back during the dark recovery stage (B).

(C) An exemplary comparison of three OCVD measurements that show the two photo-induced changes in the decay rate and the buildup of an electrostatic potential, V_{elec}.

unchanged during light soaking (full experimental details are shown in the Supplemental Information).

The OCVD data of a perovskite solar cell with a $TiO_2/CH_3NH_3PbI_{3-x}Cl_x$ interface are shown for both the light-soaking and dark recovery stages (Figures 2A and 2B, respectively). All photovoltage values in both stages were in the order of ~1.02–1.06 V, as expected from these types of cells.[16] These devices showed an average efficiency of ~15%, and an exemplary *J-V* curve of such a device is seen in Figure S1B. The decay of the reference measurement (black curve, Figure 2A) displays a similar pattern to previous findings.[14] However, when the OCVDs were examined in the light-soaking stage, two distinctive changes appeared, and these were clearly affected by the light-soaking duration. The first change was a very fast increase in the decay rate manifested as a rapid drop in the decay curves, which is counterintuitive because faster decay rates imply faster recombination—the opposite of what occurs in hybrid perovskite solar cells.[17] The second observed change was a buildup of an electrostatic potential (V_{elec}), which is defined later. In brief, the electrostatic photopotential corresponds to a displacement of the majority carrier energy level beyond the flat-band potential, forming an accumulation region. As noted in Figure 2, the electrostatic potential was very pronounced in the dark with an additional ~150 mV to the open-circuit voltage. During the illumination (red LED pulse), a smaller contribution (~20–50 mV) to the photovoltage was seen. We also note that OCVD measurements performed after shorter light-soaking times (30–90 s) have shown similar effects but are slightly less pronounced. In the dark recovery stage, the changes showed full reversibility. However, the return back to the reference values was slower, especially for V_{elec}, which took at least 60 min to full recovery, whereas the reversibility of the decay rate was slightly faster. Figure 2C compares three OCVD measurements (reference, light soaking for 6 min, and dark recovery for 60 min), showing the two dynamic photo-induced changes.

Photovoltage decays are presented in Figure 3 in terms of the instantaneous relaxation time, which has been previously defined[14] as

$$\tau_{ir}(V) = \left(-\frac{1}{V}\frac{dV}{dt} \right)^{-1}. \qquad \text{(Equation 1)}$$

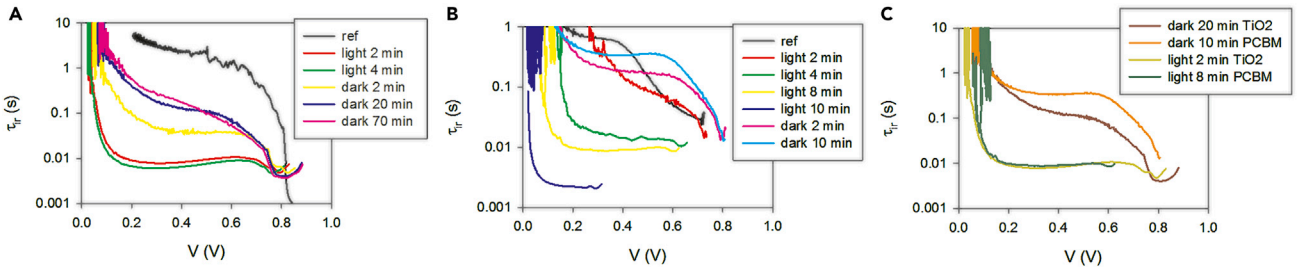

Figure 3. The Instantaneous Relaxation Times of Perovskite Solar Cells with a Structure of FTO/Compact TiO_2/mp-TiO_2/$CH_3NH_3PbI_{3-x}Cl_x$/spiro/Ag

Relaxation times were obtained from OCVD under different conditions.

(A) Cell with only TiO_2 contact.

(B) Cell with a PCBM interlayer at TiO_2 contact.

(C) Comparison of both cells.

This relaxation time is a constant when the voltage decay obeys an exponential decay. The first feature we noticed in the experiment is a qualitative difference between the shapes of the decays for a device that was stored in the dark (reference) and a device measured in the light-soaking stage (pre-illuminated). The reference showed a power law (nonexponential) decay that decreased in the range of 10–1 s, similarly to all the samples previously investigated in a different study.[14] However, when the device was pre-illuminated, the relaxation time became nearly constant with a much lower value of 0.001 s, in excellent agreement with the values reported by Sepalage et al.[18] for a solar cell with a CuI contact. The decrease in relaxation time due to the effect of pre-illumination was about two orders of magnitude. In Figure S1C, the OCVD data of devices with a PCBM interlayer are compared with the OCVD data of devices with a TiO_2 contact. Despite lower initial photovoltages, it is apparent that these devices showed a decrease in the decay rate and that an electrostatic potential also built up under light soaking. However, a discussion regarding the subtle differences between these two systems is outside the scope of this work.

In previous studies, it was observed that the kinetic behavior of perovskite solar cells is determined to a great extent by the contact interfaces. For example, a quite different response is observed between a TiO_2 electron-selective contact and a TiO_2/C_{60} monolayer contact.[19,20] It has been accepted that ion migration is an important phenomenon determining the kinetic response of perovskite solar cells.[21–23] Significant sources of evidence are the closeness of the activation energy of transient phenomena to that of iodide migration,[24] direct observations of compositional changes,[20,25] and the large capacitance observed at low frequency in the dark, which has been interpreted as a Helmholtz capacitance caused by ion accumulation.[26–28] The last type of evidence is highly relevant for the present work, because here we analyze the consequence of progressive interfacial charging. It can be concluded that when the solar cell is set at an open-circuit voltage, significant ion migration occurs toward the interface, with the consequence that the kinetic response is drastically modified by the change of conditions at the contact. It is therefore necessary to consider the properties of the contact surfaces in detail, how they evolve under the formation of open-circuit voltage, and how they are modified by the presence and accumulation of mobile ions and ion vacancies. The ion concentration changes the interface by affecting the concentration and recombination rates of the photogenerated electronic carriers, and thus the photovoltage is expected to change and to decay depending on the conditions at the interface.

Model Simulations

According to the picture established in the previous section, advanced simulation tools become necessary for understanding the complex effects occurring at the interface. Numerical methods have been implemented before in the field of perovskite solar cells,[29–34] particularly models that explain the hysteresis in perovskite solar cells on the basis of time evolution[35,36] while emphasizing the transport characteristics in the bulk, but important aspects of the interface that require demanding computational effort were simplified or not considered. It has been well recognized that the large capacitance observed in the dark at low frequencies carries information on ion accumulation at the interface by the formation of a double-layer structure.[26,37] By interpreting the low-frequency capacitance under illumination, Zarazua et al.[28] concluded that electronic carriers accumulate at the contact, so that upward band bending is formed at high voltage. The innovation of our approach in this work was to develop simulations that simultaneously take into account (1) variable mobile ion density and (2) arbitrary conditions of band bending at the interface from depletion to accumulation, thereby allowing for degenerate statistics at the contact, including a generalized Einstein relation for mobility to diffusivity. In addition to these aspects of our simulation method, we follow the standard features for describing perovskite photovoltaic devices, i.e., drift, diffusion, generation, and recombination combined with the Poisson equation for at least three carriers (electrons, holes, and ions) and with suitable boundary conditions, namely, selective contacts for electrons and holes and blocking boundaries for ions. Our model equations and simulation procedures are outlined in the Supplemental Information.

In accumulation conditions, one cannot rely on simplified approximations of the Fermi-Dirac function. In this case, the Fermi level of carriers enters the respective band edge, and the electron (n) and hole (p) densities must be evaluated with the Fermi-Dirac 1/2 integral $\Im_{1/2}$ as follows:

$$n = N_c 2/\sqrt{\pi}\ \Im_{1/2}(-(E_c - E_{Fn})/k_B T)\,, \qquad \text{(Equation 2)}$$

$$p = N_v 2/\sqrt{\pi}\ \Im_{1/2}((E_v - E_{Fp})/k_B T)\,, \qquad \text{(Equation 3)}$$

$$\Im_{1/2}(x_F) \equiv \int_0^\infty \frac{x^{1/2}}{\exp(x - x_F) + 1} dx\,, \qquad \text{(Equation 4)}$$

where $k_B T$ is the thermal energy, N_c and N_v are effective densities of states in the conduction and valence bands, respectively, E_c and E_v are the conduction and valence band-edge energies, respectively, and E_{Fn} and E_{Fp} are the electron and hole Fermi levels, respectively.

In addition, in the case of degenerate statistics, the Einstein relationship between the diffusion coefficient D_n and mobility μ_n (or D_p and μ_p) takes the form[38]

$$D_n = \mu_n \frac{k_B T}{q} \frac{\Im_{1/2}(E_c - E_{Fn})}{\Im_{-1/2}(E_c - E_{Fn})}\,. \qquad \text{(Equation 5)}$$

Equation 5 can be simplified with the approximation[39,40]

$$D_n = \mu \frac{kT}{q}\left[1 + 0.35355\left(\frac{n}{N_c}\right) - 9.9 \times 10^{-3}\left(\frac{n}{N_c}\right)^2 + 4.45 \times 10^{-4}\left(\frac{n}{N_c}\right)^3 + \cdots\right]. \qquad \text{(Equation 6)}$$

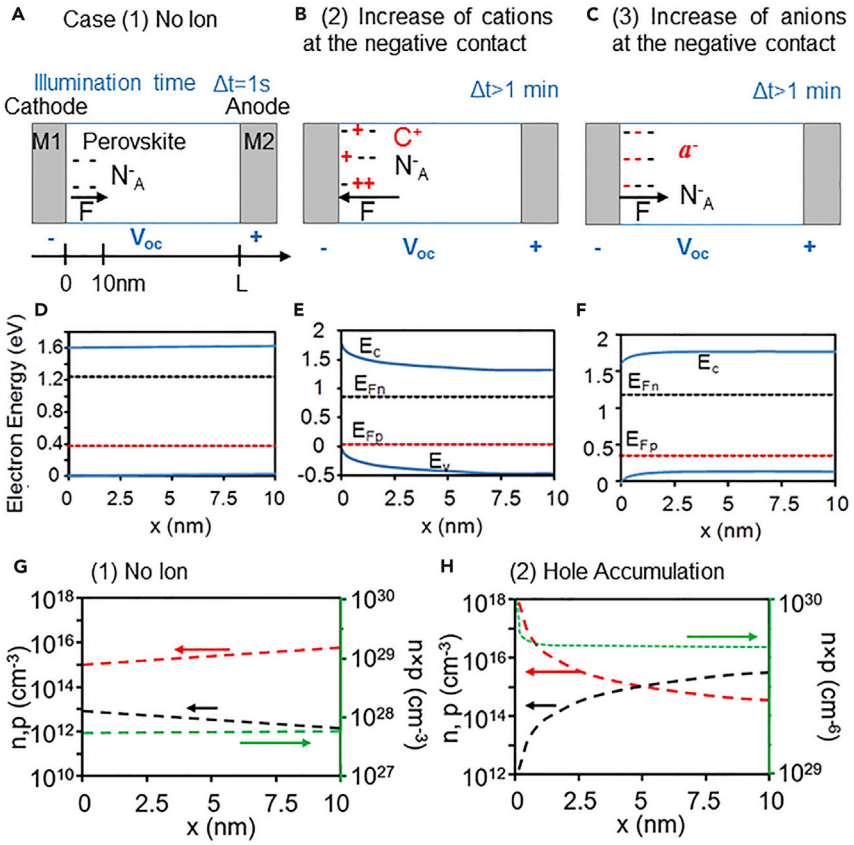

Figure 4. A Graphical Representation of the Numerical Model Simulations

(A–F) Device (A–C) and energy (D–F) diagrams of the three simulated Schottky solar cells with (1) no ions at the interface, (2) an increase in cations at the interface, and (3) an increase in anions at the interface. The parameters are detailed in Table S1.

(G and H) The hole and electron densities and the product of both densities along the first 10 nm of the cell from the negative contact for cases 1 (G) and 2 (H).

By including the above generalized statistics and Einstein relation in the simulation scheme, we are able to describe any situation from depletion to accumulation that could be induced by the additional charge that the mobile ions bring into the contact layer. This adds complexity to the numerical simulations, given that very rapidly varying band bending is formed at the interface. In order to check the convergence of the numerical results, we analyzed a test structure with a hole accumulation region, and the results are given in the Supplemental Information.

Once the numerical solution for a well-known accumulated structure was successfully tested, we analyzed the perovskite solar cell measured in Figure 2. The results are shown in Figure 4. Here, we focused our attention on a small region of the order of 10 nm right at the surface of the TiO_2 blocking layer that represents the main site for polarization and recombination. The additional mesoporous TiO_2 structure is believed not to affect the field distribution severely, and in fact test measurements with insulating mesoporous alumina gave similar results. Interfacial and bulk carrier and field distributions were calculated under illumination at open-circuit voltage V_{oc} for three different cases: (1) no mobile ions, which served as a reference, (2) increasing cation concentration at the interface, and (3)

increasing anion concentration. The actual case found in a perovskite solar cell depends on the properties of the preferential mobile ions (which we do not describe in detail here) and the built-in field. We describe the three cases as follows.

For the no-ion case, $C(x) = 0$ and $a(x) = 0$ (Figure 4A). Figure 4D shows the band diagram near the interface of a reference solar cell with no mobile ions under illumination, and Figure 4G shows the distribution of electrons and holes. In the absence of ions, the concentration of electrons and holes is nearly symmetric, as shown in Figure 4G. The region close to the left interface is slightly depleted of holes and corresponds to a p-type semiconductor with a dopant concentration of $N_A = 10^{17}$ cm^{-3}, and a small electric field points to the right of the structure. The representation along the whole semiconductor is shown in Figure S4.

For a semiconductor with cations, $C(x = 0) = C_0 \neq 0$ (Figure 4B). When we allow a preferential concentration of cations at the cathode, then an accumulation layer of holes is formed (Figures 4H),[28] which implies a very large concentration of both holes and cations to sustain the space charge layer at the contact (Figure 4E and Figure S8). Bringing cations to the cathode makes the small electric field at the interface, which exists in the sample with no ions, change its sign and direction. The electric field attracts holes to the interface, where they accumulate. This result is in contrast to a frequent hypothesis that assumes that bringing cations to the interface forms an n-doped region with improved electron concentration; our result shows just the opposite trend. The value of the open-circuit voltage obtained in the simulation, $V_{oc} = 1.1$ V, is higher than the built-in voltage, $V_{bi} = 1$ V. The condition $V_{oc} - V_{bi} > 0$ makes the net electric field point to the left. Under this electric field, the cations can be accumulated close to the negative contact if there is enough time for them to migrate. Figure S9C shows the simulation results of such a distribution after a long migration time. Note also that a pedestrian argument could be that the negative field at the contact might attract further ionic charge to the interface in a feedback process. However, Figure 4 was obtained by rigorous solution of the transport equations for determining the physical equilibrium at the open circuit, so taking into account only one aspect, such as drift transport, can be highly misleading.

For a semiconductor with anions, $a(x = 0) = a_0 \neq 0$ (Figure 4C). Bringing anions to the cathode adds negative charges to the negative ionized acceptor impurities of the depleted region. These additional negative charges increase the electric field close to the $x = 0$ interface (Figure 4F and Figure S6A), which still points to the right. The hole depletion region is enhanced and produces an increased concentration of electrons at the interface (Figure S6B). The open-circuit voltage obtained in the simulation results is $V_{oc} = 0.88$ V, which is smaller than the built-in voltage ($V_{bi} = 1$ V). The relation $V_{oc} - V_{bi} < 0$ makes the net electric field point to the right, as in the no-ion case, and causes the anions to accumulate close to the negative contact.

The previous simulations allow us to obtain an interpretation of the dark-to-light transition caused by the presence of photogenerated carriers, and more relevant to our experiments, the simulation provides insight on the dynamics of the return to equilibrium once photogeneration is removed. We must recognize that we have characterized some static situations. A fuller description would require us to develop full simulation of the transients by combining the above method with time evolution. However, this approach is far beyond the scope of the present work because of the computational complexity, although it is an important topic for future studies. In fact, establishing precise conditions for interfacial distribution

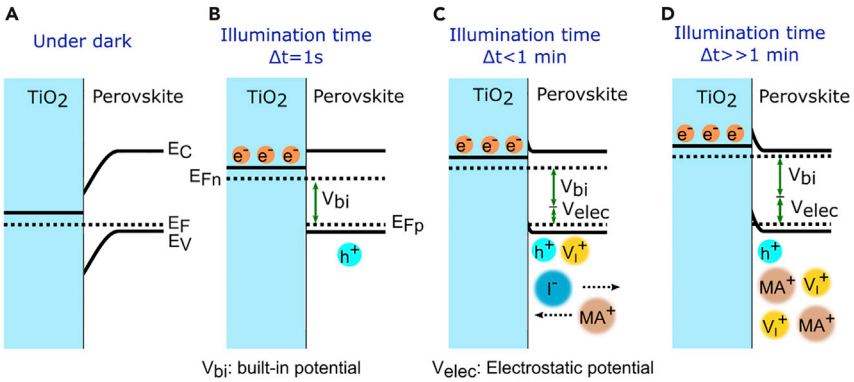

Figure 5. The Energy Diagram at the TiO_2/Perovskite Contact at Four Different Stages

(A) In the dark without migrating positive cations and vacancies.

(B) At a very short illumination time of Δt = 1 s.

(C) At an illumination time close to 1 min.

(D) After a substantial illumination time of $\Delta t \gg 1$ min. The band bending results from an increase in the hole concentration at the interface, which forms an electrostatic potential as a result of the electric field across the interface. This potential is added to the built-in potential.

already requires complex simulation work, as described above. Nevertheless, we have explored a range of features of the origin of dynamic phenomena. In general, in a perovskite solar cell, there can be several types of ions and defects moving simultaneously. The study presented here for one type of ion can be applied to samples where both cations and anions, as well as ionic vacancies, are detected. We have also studied these cases, although they do not add different conclusions to those presented above. In the case where both types of ions are present in the semiconductor, the dominant species tends to accumulate at the cathode interface. The distribution of electrons, holes, and band bending remains qualitatively the same as in the case of a unique species of ion in the semiconductor. The most significant difference is that the resulting electric field under the open-voltage condition makes the other species migrate to the opposite interface. The simulation case of Figure 4B is in agreement with the observed large photovoltage and light-induced accumulation capacitance;[28] therefore, this is the basis for the following discussion.

DISCUSSION

We have shown that the migration of ions in perovskite can have a significant effect on perovskite-based devices, particularly as a result of ion accumulation at the contacts. Let us consider the implications of the model just described for the interpretation of experimental results and illustrate the energy diagram of the TiO_2/perovskite interface under different conditions (Figure 5). After a long dark storage period, the state of the system is shown in Figure 5A. The height of the Schottky barrier at the TiO_2/perovskite interface (the total band bending) has the value $V_{bi} = \Phi_1 - E_{F0}$ in terms of the work function of TiO_2 Φ_1 and the Fermi level in the bulk perovskite layer (Figure S2A). We have assumed that band bending inside TiO_2 and at the anode is negligible. It is possible to adopt more realistic conditions as previously reported,[41] but such detailed description lies outside the scope of this work. When the cell is illuminated, it takes time to construct the steady-state distribution (Figure 4H). Thus, upon illumination (e.g., Δt = 1 s), the energy diagram at the TiO_2/perovskite interface can be described as in Figure 5B. The charging time of the interface can take several minutes and is described as a slow change from Figures 5B to 5C (Δt < 1 min). Therefore, the actual distribution of carriers at the interface evolves

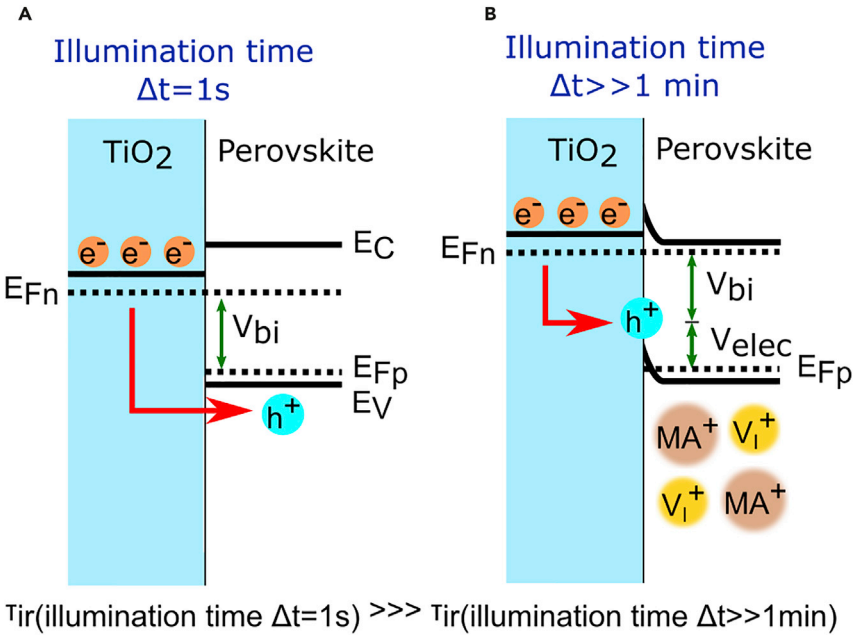

Figure 6. The Energy Diagram at the TiO_2/Perovskite Contact at Two Different Stages

(A) At a very short illumination time (red LED pulse only) of Δt = 1 s.

(B) After a substantial light-soaking time of $\Delta t \gg 1$ min.

The recombination in both cases is orders of magnitude different as a result of the different hole concentration at the interface in each case, manifested by a large change in the relaxation time, τ_{ir}.

with time (as in Figures 4D and 4E). After a substantial time of light soaking ($\Delta t \gg$ 1 min), the system reaches the state seen in Figure 5D.

Also seen in Figure 5D are two important features. The first is the presence of larger hole concentration at the interface than in Figure 5B as a result of accumulation conditions.[28] The second is the new structure of band bending at the interface. At the flat-band condition in Figure 5B, the initial band bending associated with V_{bi} has been removed by the increase in the minority carrier's Fermi level, E_{Fn}. However, the minority carrier E_{Fn} can still rise further by building interfacial band bending in the contrary direction. This feature creates an additional electrostatic potential, V_{elec}, as a result of the electric field formed across the junction due to the accumulation region. This electrostatic potential is therefore added to the built-in potential and increases the overall photovoltage. In total, we have

$$V_{oc} = V_{bi} + V_{elec} \,. \qquad \text{(Equation 7)}$$

These features have important effects on the OCVD measurements and further consequences for other characterization techniques of contact/perovskite systems. Here, we explain our interpretation of these two features, starting with the high concentration of holes at the interface after long illumination times.

When OCVD is measured on a device that is in a similar state as in Figure 5D, rapid recombination occurs at the interface upon light removal because of the large concentration of carriers on both sides. This was seen in Figure 3, where the relaxation time decreased by two orders of magnitude after a light-soaking period. This rapid recombination is illustrated in Figure 6, which shows the large difference in τ_{ir} between the two extreme cases: a short illumination time of Δt = 1 s (only red LED pulse) versus a long light-soaking duration of $\Delta t \gg 1$ min. This feature suggests

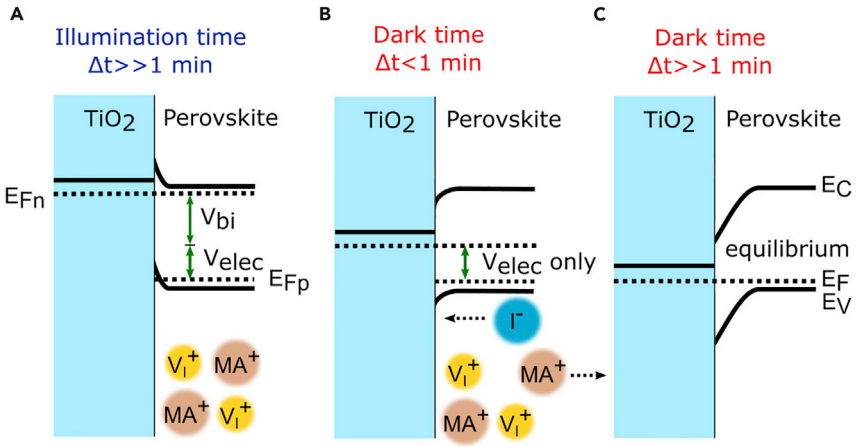

Figure 7. The Dark Recovery Process after Prolonged Light Soaking

The energy diagram at the TiO_2/perovskite contact after a substantial light-soaking time of $\Delta t \gg 1$ min (A), the slow return to the steady state without migrating ions (B), and a dark recovery time of $\Delta t \gg 1$ min (C).

that the actual device is not being measured but that what is being measured in practice is the recombination at the contact/perovskite interface. This interface recombination can be explained by the quantity $np - n_i^2$, which determines how far the semiconductor is from reaching equilibrium, which is several orders of magnitude greater in the sample containing cations (Figure 4H) than in the sample with no ions (Figure 4G). Although this quantity increases throughout the entire semiconductor, the increment is important at the interface where holes accumulate. This change means that the transient quasi Fermi level of electrons is not homogeneous in the solar cell, and the contact predominantly detects the Fermi level right at this place. As a result, the decrease in photovoltage (when the light is turned off) over time is strictly determined by the Fermi level in the contact itself.

The second feature, the additional electrostatic potential, V_{elec}, is slightly less pronounced under illumination (an additional 20–50 mV; Figure 2A) as a result of the higher recombination rate. However, once the light is turned off, and the recombination occurs in the interface, a higher value of V_{elec} is observed (~150 mV; Figure 2). This additional potential could be the reason for the high photovoltages of these materials. Figure 6A shows a scheme in which, after a long illumination time ($\Delta t \gg 1$ min), the overall potential is a combination of both contributions.

When the light is turned off (moving from Figure 7A to Figure 7B), the built-in potential drops down instantly, but the electrostatic potential still exists because of the slow migration of ions back in the dark. In this state, a substantial open-circuit voltage can be measured in the dark. The slow return to a steady state with no ion accumulation (Figure 7C) can take tens of minutes and perhaps longer, as seen in Figures 2B and 2C. Such slow timescales were also observed in free-standing perovskite films when micro-Raman and photoluminescence microscopy was used.[42,43]

Another important aspect of the experimental results is the change in the kinetic behavior determined by the contact interfaces. Indeed, a quite different response is observed between a TiO_2 electron-selective contact and a TiO_2/C_{60} monolayer contact. It has been previously reported that this modification introduces major changes in the amount of current-voltage hysteresis[44] and in the charge-transfer

kinetics across the contact.[19] In addition, the recombination at interface traps has been identified as a major site, causing current-voltage hysteresis.[35] Similarly, we observed a considerable difference in the light-soaking time dependence of the relaxation time when a PCBM interlayer was deposited on mp-TiO_2. Apparently, if the PCBM contact is left for a longer pre-illumination time, it achieves the same τ_{ir} as the TiO_2 contact. Similar results, in which the two types of contact tend to the same behavior, have been reported before.[19,20] The modeling reported here does not allow for a detailed description of the atomistic structure of the interface. In principle, we attribute the different kinetic behaviors to variation in the interfacial conditions. The presence of a thin organic layer introduces a significant difference with respect to TiO_2/perovskite contact by smoothing the interface and removing voids and provides an additional layer that can easily absorb the excess ions. The strong changes in low-frequency capacitance[3] point in the direction that the charge accumulation is reduced, modifying the kinetic properties as well. The accumulation of ionic-electronic charge at the electron contact exerts a strong influence in terms of important measurements, such as the *J-V* curve, which has a transient component that frequently causes hysteresis to a larger or lesser extent. Indeed, as we showed that a large quantity of charge is accumulated and removed at the interface, it provides a transient current that is not simply instantaneous capacitive current[45] because it is modulated by relaxation of the interfacial charge. This complex behavior will be the topic of separate studies.

After this work had been completed, we noticed that Bergmann et al.[46] had identified the charge accumulation at the electron contact by direct measurement of frequency-modulation Kelvin probe force microscopy (FM-KPFM) of the cross-section of devices. Importantly, they remark that the large global charge imbalance at both interfaces cannot be formed by ionic charge alone and is explained by the accumulation of both cations and majority holes at the electron contact. These results further support the rather counterintuitive idea that the electron extraction contact contains a huge density of positive electronic (holes) and ionic (cations) charge, rather than negative electronic charge, at the perovskite side of the interface.

Conclusions

In summary, we have studied the OCVD of lead halide perovskite solar cells. This technique is very common for the measurement of recombination lifetimes in other types of solar cells because of its simplicity, and it is representative of a different way of measuring time or frequency domain characterization in operative devices, in which Fermi levels at the contacts (and not in the bulk of the device) are measured. These observations therefore have broad indications for the interpretation of characterization techniques for perovskite solar cells. Our measurements of the voltage-decay relaxation time varied significantly, which we interpreted by using advanced physical modeling in terms of major changes in the contact region caused by light-soaking pre-treatment. Our modeling suggests that as the light-soaking time progresses, recombination (under photovoltage conditions) in the contact increases as a result of a higher accumulation of holes at the interface. When the light is turned off, rapid recombination at the interface occurs, seen as a dramatic change in the relaxation time. This is unrelated to the type of contact material; however, the type of material affects the changes in kinetics. Another important phenomenon, which results from the charge accumulation at both sides of the interface, is an electrostatic potential that is sustained by the accumulation of slow mobile ion charges in the double layer at the contact, which cause dramatically long decay times. This electrostatic component of the photovoltage goes beyond the natural built-in voltage of the interface. During illumination, the electrostatic potential somewhat

compensates for the higher recombination during open-circuit conditions, seen as an additional tens of millivolts to the photovoltage. However, once the light is removed, the magnitude of the electrostatic component is ~150 mV. Unfortunately, we have to conclude that the result of the measurement is not representative of a "bulk" or intensive quantity but rather depends drastically on the particular history of the interface. This suggests the need for detailed reanalysis of different types of measurements that require specific protocols, yet to be developed, in order to give reproducible and physically meaningful results. This implies that pre-treatments significantly change the results of characterization techniques that use contacts, meaning that any techniques that measure a full device, and anyone measuring perovskite-based solar cells, must take this information into consideration.

EXPERIMENTAL PROCEDURES

Full experimental procedures are provided in the Supplemental Information.

SUPPLEMENTAL INFORMATION

Supplemental Information includes Supplemental Experimental Procedures and ten figures and can be found with this article online at http://dx.doi.org/10.1016/j.chempr.2016.10.002.

AUTHOR CONTRIBUTIONS

Conceptualization, J.B., L.G., R.G., and A.Z.; Formal Analysis, R.G., J.J.-T., P.L.-V., and S.T.; Investigation, L.G., R.G., J.H., P.L.-V., and S.T.; Writing – Original Draft, J.B., R.G., and P.L.-V.; Writing – Review & Editing, J.B., R.G., P.L.-V., and A.Z.; Funding Acquisition, J.B. and A.Z.; Resources, J.B., J.A., J.-T., and A.Z.; Supervision, J.B. and A.Z.

ACKNOWLEDGMENTS

The work was supported by MINECO of Spain under projects MAT2013-47192-C3-1-R and TEC2013-47283-R and grant FPU12/02712, the Israeli National Nanotechnology Initiative (INNI, FTA project), the Israel Strategic Alternative Energy Foundation (I-SAEF), and the "Tashtiyot" Program of the Israeli Ministry of Science & Technology. L.G. acknowledges financial support from the European Union Seventh Framework Program Destiny Project under grant 316494.

Received: August 14, 2016
Revised: September 8, 2016
Accepted: October 4, 2016
Published: November 10, 2016

REFERENCES AND NOTES

1. Snaith, H.J., Abate, A., Ball, J.M., Eperon, G.E., Leijtens, T., Noel, N.K., Stranks, S.D., Wang, J.T.-W., Wojciechowski, K., and Zhang, W. (2014). Anomalous hysteresis in perovskite solar cells. J. Phys. Chem. Lett. *5*, 1511–1515.

2. Unger, E.L., Hoke, E.T., Bailie, C.D., Nguyen, W.H., Bowring, A.R., Heumuller, T., Christoforo, M.G., and McGehee, M.D. (2014). Hysteresis and transient behavior in current-voltage measurements of hybrid-perovskite absorber solar cells. Energy Environ. Sci. *7*, 3690–3698.

3. Kim, H.-S., Jang, I.-H., Ahn, N., Choi, M., Guerrero, A., Bisquert, J., and Park, N.-G. (2015). Control of I-V hysteresis in CH3NH3PbI3 perovskite solar cell. J. Phys. Chem. Lett. *6*, 4633–4639.

4. Sanchez, R.S., Gonzalez-Pedro, V., Lee, J.-W., Park, N.-G., Kang, Y.S., Mora-Sero, I., and Bisquert, J. (2014). Slow dynamic processes in lead halide perovskite solar cells. Characteristic times and hysteresis. J. Phys. Chem. Lett. *5*, 2357–2363.

5. Gottesman, R., Haltzi, E., Gouda, L., Tirosh, S., Bouhadana, Y., Zaban, A., Mosconi, E., and De Angelis, F. (2014). Extremely slow photoconductivity response of CH3NH3PBI3 perovskites suggesting structural changes under working conditions. J. Phys. Chem. Lett. *5*, 2662–2669.

6. Gottesman, R., and Zaban, A. (2016). Perovskites for photovoltaics in the spotlight: photoinduced physical changes and their implications. Acc. Chem. Res. *49*, 320–329.

7. Shi, J., Xu, X., Li, D., and Meng, Q. (2015). Interfaces in perovskite solar cells. Small *11*, 2472–2486.

8. Fan, R., Huang, Y., Wang, L., Li, L., Zheng, G., and Zhou, H. (2016). The progress of interface

design in perovskite-based solar cells. Adv. Energy Mater. *6*, 1600460.

9. Schulz, P., Edri, E., Kirmayer, S., Hodes, G., Cahen, D., and Kahn, A. (2014). Interface energetics in organo-metal halide perovskite-based photovoltaic cells. Energy Environ. Sci. *7*, 1377–1381.

10. Zaban, A., Greenshtein, M., and Bisquert, J. (2003). Determination of the electron lifetime in nanocrystalline dye solar cells by open-circuit voltage decay measurements. ChemPhysChem *4*, 859–864.

11. Palomares, E., Clifford, J.N., Haque, S.A., Lutz, T., and Durrant, J.R. (2003). Control of charge recombination dynamics in dye sensitized solar cells by the use of conformally deposited metal oxide blocking layers. J. Am. Chem. Soc. *125*, 475.

12. Wang, L., McCleese, C., Kovalsky, A., Zhao, Y., and Burda, C. (2014). Femtosecond time-resolved transient absorption spectroscopy of CH3NH3PbI3 perovskite films: evidence for passivation effect of PbI2. J. Am. Chem. Soc. *136*, 12205–12208.

13. Yuan, Y., and Huang, J. (2016). Ion migration in organometal trihalide perovskite and its impact on photovoltaic efficiency and stability. Acc. Chem. Res. *49*, 286–293.

14. Bertoluzzi, L., Sanchez, R.S., Liu, L., Lee, J.-W., Mas-Marza, E., Han, H., Park, N.-G., Mora-Sero, I., and Bisquert, J. (2015). Cooperative kinetics of depolarization in CH3NH3PbI3 perovskite solar cells. Energy Environ. Sci. *8*, 910–915.

15. Gouda, L., Gottesman, R., Tirosh, S., Haltzi, E., Hu, J., Ginsburg, A., Keller, D.A., Bouhadana, Y., and Zaban, A. (2016). Vapor and healing treatment for CH3NH3PbI3-xClx films toward large-area perovskite solar cells. Nanoscale *8*, 6386–6392.

16. Harwell, J.R., Baikie, T.K., Baikie, I.D., Payne, J.L., Ni, C., Irvine, J.T.S., Turnbull, G.A., and Samuel, I.D.W. (2016). Probing the energy levels of perovskite solar cells via Kelvin probe and UV ambient pressure photoemission spectroscopy. Phys. Chem. Chem. Phys. *18*, 19738–19745.

17. Frost, J.M., Butler, K.T., and Walsh, A. (2014). Molecular ferroelectric contributions to anomalous hysteresis in hybrid perovskite solar cells. APL Mater. *2*, 081506.

18. Sepalage, G.A., Meyer, S., Pascoe, A., Scully, A.D., Huang, F., Bach, U., Cheng, Y.-B., and Spiccia, L. (2015). Copper(I) iodide as hole-conductor in planar perovskite solar cells: probing the origin of J–V hysteresis. Adv. Funct. Mater. *25*, 5650–5661.

19. Tao, C., Neutzner, S., Colella, L., Marras, S., Srimath Kandada, A.R., Gandini, M., Bastiani, M.D., Pace, G., Manna, L., Caironi, M., et al. (2015). 17.6% stabilized efficiency in low-temperature processed planar perovskite solar cells. Energy Environ. Sci. *8*, 2365–2370.

20. De Bastiani, M., Dell'Erba, G., Gandini, M., D'Innocenzo, V., Neutzner, S., Kandada, A.R.S., Grancini, G., Binda, M., Prato, M., Ball, J.M., et al. (2016). Ion migration and the role of preconditioning cycles in the stabilization of the J–V characteristics of inverted hybrid perovskite solar cells. Adv. Energy Mater. *6*, 1501453.

21. Xiao, Z., Yuan, Y., Shao, Y., Wang, Q., Dong, Q., Bi, C., Sharma, P., Gruverman, A., and Huang, J. (2015). Giant switchable photovoltaic effect in organometal trihalide perovskite devices. Nat. Mater. *14*, 193–198.

22. Yang, T.-Y., Gregori, G., Pellet, N., Grätzel, M., and Maier, J. (2015). The significance of ion conduction in a hybrid organic–inorganic lead-iodide-based perovskite photosensitizer. Angew. Chem. Int. Ed. Engl. *54*, 7905–7910.

23. Azpiroz, J.M., Mosconi, E., Bisquert, J., and De Angelis, F. (2015). Defect migration in methylammonium lead iodide and its role in perovskite solar cell operation. Energy Environ. Sci. *8*, 2118–2127.

24. Eames, C., Frost, J.M., Barnes, P.R.F., O/'Regan, B.C., Walsh, A., and Islam, M.S. (2015). Ionic transport in hybrid lead iodide perovskite solar cells. Nat. Commun. *6*, 7497.

25. Li, C., Tscheuschner, S., Paulus, F., Hopkinson, P.E., Kießling, J., Köhler, A., Vaynzof, Y., and Huettner, S. (2016). Iodine migration and its effect on hysteresis in perovskite solar cells. Adv. Mater. *28*, 2446–2454.

26. Almora, O., Guerrero, A., and Garcia-Belmonte, G. (2016). Ionic charging by local imbalance at interfaces in hybrid lead halide perovskites. Appl. Phys. Lett. *108*, 043903.

27. Guerrero, A., Garcia-Belmonte, G., Mora-Sero, I., Bisquert, J., Kang, Y.S., Jacobsson, T.J., Correa-Baena, J.-P., and Hagfeldt, A. (2016). Properties of contact and bulk impedances in hybrid lead halide perovskite solar cells including inductive loop elements. J. Phys. Chem. C *120*, 8023–8032.

28. Zarazua, I., Bisquert, J., and Garcia-Belmonte, G. (2016). Light-induced space-charge accumulation zone as photovoltaic mechanism in perovskite solar cells. J. Phys. Chem. Lett. *7*, 525–528.

29. Minemoto, T., and Murata, M. (2014). Device modeling of perovskite solar cells based on structural similarity with thin film inorganic semiconductor solar cells. J. Appl. Phys. *116*, 054505.

30. Liu, F., Zhu, J., Wei, J., Li, Y., Lv, M., Yang, S., Zhang, B., Yao, J., and Dai, S. (2014). Numerical simulation: toward the design of high-efficiency planar perovskite solar cells. Appl. Phys. Lett. *104*, 253508.

31. Foster, J.M., Snaith, H.J., Leijtens, T., and Richardson, G. (2014). A model for the operation of perovskite based hybrid solar cells: formulation, analysis, and comparison to experiment. SIAM J. Appl. Math. *74*, 1935–1966.

32. Tress, W., Marinova, N., Moehl, T., Zakeeruddin, S.M., Nazeeruddin, M.K., and Gratzel, M. (2015). Understanding the rate-dependent J-V hysteresis, slow time component, and aging in CH3NH3PbI3 perovskite solar cells: the role of a compensated electric field. Energy Environ. Sci. *8*, 995–1004.

33. Zhou, Y., and Gray-Weale, A. (2016). A numerical model for charge transport and energy conversion of perovskite solar cells. Phys. Chem. Chem. Phys. *18*, 4476–4486.

34. Miyano, K., Tripathi, N., Yanagida, M., and Shirai, Y. (2016). Lead halide perovskite photovoltaic as a model p–i–n diode. Acc. Chem. Res. *49*, 303–310.

35. van Reenen, S., Kemerink, M., and Snaith, H.J. (2015). Modeling anomalous hysteresis in perovskite solar cells. J. Phys. Chem. Lett. *6*, 3808–3814.

36. Richardson, G., O'Kane, S.E.J., Niemann, R.G., Peltola, T.A., Foster, J.M., Cameron, P.J., and Walker, A.B. (2016). Can slow-moving ions explain hysteresis in the current-voltage curves of perovskite solar cells? Energy Environ. Sci. *9*, 1476–1485.

37. Almora, O., Zarazua, I., Mas-Marza, E., Mora-Sero, I., Bisquert, J., and Garcia-Belmonte, G. (2015). Capacitive dark currents, hysteresis, and electrode polarization in lead halide perovskite solar cells. J. Phys. Chem. Lett. *6*, 1645–1652.

38. Landsberg, P.T. (1981). Einstein and statistical thermodynamics. III. The diffusion-mobility relation in semiconductors. Eur. J. Phys. *2*, 213.

39. Sze, S.M. (1981). Physics of Semiconductor Devizes, Second Edition (John Wiley).

40. Kroemer, H. (1978). The Einstein relation for degenerate carrier concentrations. IEEE Trans. Electron Devices *25*, 850.

41. Guerrero, A., Juarez-Perez, E.J., Bisquert, J., Mora-Sero, I., and Garcia-Belmonte, G. (2014). Electrical field profile and doping in planar lead halide perovskite solar cells. Appl. Phys. Lett. *105*, 133902.

42. Gottesman, R., Gouda, L., Kalanoor, B.S., Haltzi, E., Tirosh, S., Rosh-Hodesh, E., Tischler, Y., Zaban, A., Quarti, C., Mosconi, E., and De Angelis, F. (2015). Photoinduced reversible structural transformations in free-standing CH3NH3PbI3 perovskite films. J. Phys. Chem. Lett. *6*, 2332–2338.

43. deQuilettes, D.W., Zhang, W., Burlakov, V.M., Graham, D.J., Leijtens, T., Osherov, A., Bulovic, V., Snaith, H.J., Ginger, D.S., and Stranks, S.D. (2016). Photo-induced halide redistribution in organic-inorganic perovskite films. Nat. Commun. *7*, 11683.

44. Wojciechowski, K., Stranks, S.D., Abate, A., Sadoughi, G., Sadhanala, A., Kopidakis, N., Rumbles, G., Li, C.-Z., Friend, R.H., Jen, A.K.Y., and Snaith, H.J. (2014). Heterojunction modification for highly efficient organic–inorganic perovskite solar cells. ACS Nano *8*, 12701–12709.

45. Garcia-Belmonte, G., and Bisquert, J. (2016). Distinction between capacitive and noncapacitive hysteretic currents in operation and degradation of perovskite solar cells. ACS Energy Lett. *1*, 683–688.

46. Bergmann, V.W., Guo, Y., Tanaka, H., Hermes, I.M., Li, D., Klasen, A., Bretschneider, S.A., Nakamura, E., Berger, R., and Weber, S.A.L. (2016). Local time-dependent charging in a perovskite solar cell. ACS Appl. Mater. Inter. *8*, 19402–19409.